

# Cooling of photoexcited carriers in graphene by internal and substrate phonons

Tony Low,<sup>1</sup> Vasili Perebeinos,<sup>1</sup> Raseong Kim,<sup>2,\*</sup> Marcus Freitag,<sup>1</sup> and Phaedon Avouris<sup>1</sup>

<sup>1</sup>IBM T.J. Watson Research Center, Yorktown Heights, New York 10598, USA

<sup>2</sup>Network for Computational Nanotechnology, Purdue University, West Lafayette, Indiana 47907, USA

(Received 4 June 2012; published 9 July 2012)

We investigate the energy relaxation of hot carriers produced by photoexcitation of graphene through coupling to both intrinsic and remote (substrate) surface polar phonons using the Boltzmann equation approach. We find that the energy relaxation of hot photocarriers in graphene on commonly used polar substrates, under most conditions, is dominated by remote surface polar phonons. We also calculate key characteristics of the energy relaxation process, such as the transient cooling time and steady-state carrier temperatures and photocarrier densities, which determine the thermoelectric and photovoltaic photoresponse, respectively. Substrate engineering can be a promising route to efficient optoelectronic devices driven by hot carrier dynamics.

DOI: [10.1103/PhysRevB.86.045413](https://doi.org/10.1103/PhysRevB.86.045413)

PACS number(s): 78.67.Wj, 78.20.Bh, 72.20.Jv, 72.80.Vp

## I. INTRODUCTION

Upon fast excitation of graphene carriers with light or other means, the dynamics of the resulting nonequilibrium carrier distribution evolves on a fast time scale and has been extensively studied both experimentally<sup>1–13</sup> and theoretically.<sup>14–16</sup> The relaxation involves an initial fast evolution towards quasithermal distribution on a femtosecond time scale via electron-electron collisions,<sup>14,15,17,18</sup> followed by energy transfer to phonons on a longer picosecond time scale. The conversion of the excess energy of these photoexcited carriers into electrical current before they lose this energy to the phonon baths represents one of the key challenges to efficient optoelectronic device.

In this paper, we study the energy relaxation pathways of the photoexcited carriers via different inelastic scattering channels. Energy relaxation processes in graphene due to intrinsic optical and acoustic phonons have already been studied.<sup>15,19–21</sup> High-energy optical phonon emission by hot carriers is responsible for the subpicosecond fast cooling process,<sup>1,2,22</sup> followed by cooling via the acoustic modes. The latter is a slow process, which creates an electron-phonon cooling bottleneck.<sup>19</sup> Here, we focus on an extrinsic mechanism for cooling of photoexcited carriers in graphene via the remote surface polar phonon modes (SPP) of the substrate and compare their efficiency under different conditions with those of the internal phonon modes.

In polar substrates such as SiO<sub>2</sub>, a nonvanishing fluctuating electric field is generated by the propagating surface phonon modes.<sup>23</sup> The interactions of these SPP modes with charged carriers in the conduction channel was first explored in the context of inversion layer of semiconductor-oxide interface.<sup>24–26</sup> They have also been studied in other material systems such as carbon nanotubes,<sup>27–29</sup> where close proximity between charged carriers and the underlying substrate renders the SPP phonon scattering more prominent. Similarly, in graphene, SPP was found to limit electronic transport properties.<sup>30–39</sup> Recently, the SPP coupling with graphene plasmons was also probed experimentally through infrared spectroscopy.<sup>40–42</sup> In this work, we found irrespectively of the mechanism, i.e., thermoelectric or photovoltaic, that SPP limits the overall strength of the steady-state photoresponse on common substrates, and our results suggest that elimination of the SPP cooling channel can lead to an order-of-magnitude enhancement in the photoresponse.

In Sec. II, we present the general theory, while details of the models for the electron cooling power via the different phonon baths are presented in the Appendixes. We present the results of our calculation of the cooling powers in Sec. III A and discuss their relative contribution in detail, as a function of doping and electronic/lattice temperatures. In Sec. III B, we apply the above models to the study of the cooling dynamics of hot carriers due to continuous or pulsed light excitations. We calculate key experimental observables such as the transient cooling time, and steady-state quantities such as the nonequilibrium electronic temperatures, excess photocarrier density, and the out-of-plane thermal conductivity for graphene on common substrates.

## II. THEORY AND MODELS

Transition probability for emission and absorption of phonons with a particular phonon bath  $\alpha$  is described by Fermi's golden rule

$$S_{\alpha}(\mathbf{k}, \mathbf{k}') = \frac{2\pi}{\hbar} \sum_{\mathbf{q}} \frac{1}{A} |M_{\mathbf{k}, \mathbf{k}'}^{\alpha}|^2 \{ N_{\omega_q} \delta_{\mathbf{k}' - \mathbf{k} - \mathbf{q}} \delta(E_{\mathbf{k}'} - E_{\mathbf{k}} - \hbar\omega_q) + (N_{\omega_q} + 1) \delta_{\mathbf{k}' - \mathbf{k} + \mathbf{q}} \delta(E_{\mathbf{k}'} - E_{\mathbf{k}} + \hbar\omega_q) \}, \quad (1)$$

where  $\mathbf{q}$  is the phonon momentum,  $N_{\omega_q} = [\exp(\hbar\omega_q/k_B T_L) - 1]^{-1}$  is the Bose-Einstein distribution, and  $M_{\mathbf{k}, \mathbf{k}'}^{\alpha}$  are the transition matrix elements related to the coupling with phonon bath  $\alpha$ , to be defined in the following. For brevity, summation  $\sum_{\mathbf{q}} \delta_{\mathbf{k}' - \mathbf{k} \pm \mathbf{q}}$  shall be implicit hereafter. The cooling power is computed numerically by accounting for the transfer of electronic energy to the lattice during each scattering event, i.e.,  $E_{\mathbf{k}} - E_{\mathbf{k}'}$ . Therefore, the net cooling power is calculated via<sup>19,21,43,44</sup>

$$\begin{aligned} \mathcal{P}_{ss'}^{\alpha} &= \frac{g_s g_v}{A} \sum_{\mathbf{k}} \sum_{\mathbf{k}'} S_{\alpha}(\mathbf{k}, \mathbf{k}') (E_{\mathbf{k}} - E_{\mathbf{k}'}) f_{\mathbf{k}} (1 - f_{\mathbf{k}'}) \\ &= \frac{2\pi g_s g_v}{\hbar A^2} \sum_{\mathbf{k}, \mathbf{k}'} |M_{\mathbf{k}, \mathbf{k}'}^{\alpha}|^2 \delta(E_{\mathbf{k}'} - E_{\mathbf{k}} - \hbar\omega_q) \\ &\quad \times (E_{\mathbf{k}'} - E_{\mathbf{k}}) \mathcal{F}(k, k') \\ &= \frac{g_s g_v}{(2\pi)^2 \hbar} \int_0^{\infty} k dk \int_0^{\infty} k' dk' \int_0^{2\pi} d\theta |M_{\mathbf{k}, \mathbf{k}'}^{\alpha}|^2 \\ &\quad \times \delta(k' - k - \omega_q v_F^{-1}) (k' - k) \mathcal{F}(k, k'), \end{aligned} \quad (2)$$

where  $T_L$  and  $T_E$  are the lattice and electron temperatures, respectively, and the electron distribution function is described by  $f_{\mathbf{k}}$ , and we define a composite Fermi-boson distribution function as

$$\mathcal{F}(k, k') \equiv (N_{\omega_q} + 1) f_{\mathbf{k}'}(1 - f_{\mathbf{k}}) - N_{\omega_q} f_{\mathbf{k}}(1 - f_{\mathbf{k}'}). \quad (3)$$

As indicated by experiments,<sup>1,2,18</sup> the electronic system is thermalized by the electron-electron interactions which occur at much faster time scale than the electron-phonon processes we are calculating here. Hence, it is appropriate to simply assume that  $f_{\mathbf{k}}$  follows the Fermi-Dirac distribution function, i.e.,  $\{1 + \exp[\beta(E_{\mathbf{k}} - \mu)]\}^{-1}$  where  $\beta = 1/k_B T_E$  and  $\mu$  is the chemical potential, controlled by chemical doping or electrical gating in experiments. It is apparent that the composite electron-phonon distribution function  $\mathcal{F}(k, k')$  becomes zero when  $T_E = T_L$ , hence zero cooling power.

In this work, we are interested in the energy exchange of electrons with the different phonon baths, i.e., intrinsic acoustic phonons (AP), optical phonons (OP), and surface phonon polaritons (SPP). Vibrations of the substrate ions with the opposite charge polarity produce an electric field which decays exponentially away from the surface. Carriers in the nearby graphene can feel this electric field and be scattered by the SPP phonon. The decay length of the electric field is determined by the momentum transfer in the electron-phonon scattering event. For typical carrier density in graphene, the relevant momentum transfer is of the order of  $\text{nm}^{-1}$ , such that a substantial coupling strength is expected for graphene placed at van der Waals distance of  $3.4 \text{ \AA}$  away from the

TABLE I. Parameters for the optical (OP), acoustic (AP), and substrate phonons (SPP). For SPP, we consider  $\text{SiO}_2$  and  $h$ -BN substrates.  $\epsilon_{\text{low}}$  ( $\epsilon_{\text{high}}$ ) is the low- (high-) frequency dielectric constant of the dielectric and the surface optical phonon (SO) energies are obtained from the bulk longitudinal optical phonon (LO) phonons as  $\hbar\omega_{\text{SO}} = \hbar\omega_{\text{LO}} \left( \frac{1 + 1/\epsilon_{\text{low}}}{1 + 1/\epsilon_{\text{high}}} \right)^{1/2}$ . In this work, we consider only the two SO modes with the strongest coupling strength, denoted as  $\omega_1$  and  $\omega_2$ .  $F_j$  is the electron coupling parameter with the SO modes. For internal phonon modes, the energies of OP ( $\Gamma$  and K) and their deformation potential  $D_{op}$  used in this work are summarized, and the sound velocity  $v_s$  and deformation potential for the AP mode  $D_{ac}$ . See also the respective Appendix for details.

SPP	$\text{SiO}_2$ (Ref. 33)	$h$ -BN (Ref. 48)
$\epsilon_{\text{low}}$	3.9	5.09
$\epsilon_{\text{high}}$	2.4	4.1
$\hbar\omega_1$ (meV)	58.9	101.7
$\hbar\omega_2$ (meV)	156.4	195.7
$F_1^2$ (meV)	0.237	0.258
$F_2^2$ (meV)	1.612	0.52
OP		
	$\Gamma$	K
$D_{op}$ (eV $\text{\AA}^{-1}$ )	11	16
$\hbar\omega_0$ (meV)	197	157
AP		
$D_{ac}$ (eV)	7.1	
$v_s$ (km/s)	17	

substrate. The transition matrix elements  $M_{\mathbf{k}, \mathbf{k}'}^\alpha$  for electron interaction with AP, OP, and SPP phonons are well known in the literatures.<sup>26,32,33,45-47</sup> We therefore defer their discussions to the Appendixes, with the parameter set summarized in Table I. We shall focus on the key results in what follows.

### III. RESULTS AND DISCUSSIONS

#### A. Competing cooling pathways

We begin with a simple illustration of the possible cooling pathways for photoexcited carriers in graphene in Fig. 1. Each thermal bath can be characterized by their respective temperatures  $T_\alpha$ , and are in general different from the ambient temperature  $T_0$ . The heat exchange between these thermal baths can be described by the thermal conductivity  $\kappa$ , defined as the ratio between the power exchange per unit temperature difference, i.e.,  $\delta P / \delta T$ . In general, the different phonon baths can each establish a different temperature upon interactions with the electrons (see also discussion in Sec. III B). In this work, we shall assume a common temperature for all these phonon baths, denoted simply as the lattice temperature  $T_L$ .

For a typical  $\text{SiO}_2$  substrate thickness of  $h = 50\text{--}300 \text{ nm}$ ,  $\kappa_0 = \kappa/h$  varies in a range  $\approx 5 \text{ MW/Km}^2\text{--}10 \text{ MW/Km}^2$ , where  $\text{SiO}_2$  film thermal conductivity is  $\kappa = 0.5\text{--}1.4 \text{ W/mK}$ .<sup>49</sup> The interface thermal conductance of graphene on  $\text{SiO}_2$  substrate has been measured using various experimental techniques,<sup>50-54</sup> with values ranging from  $\approx 25 \text{ MW/Km}^2\text{--}180 \text{ MW/Km}^2$ . On the theory front, several approaches have been employed to estimate this interface thermal conductance,<sup>55-59</sup> which varies from  $\approx 1 \text{ MW/Km}^2\text{--}100 \text{ MW/Km}^2$ . As illustrated in Fig. 1, energy transferred from electrons to the internal phonon baths is conducted to the underlying substrate through a phonon-limited  $\kappa_{\text{TB}}$ .  $\kappa_{\text{TB}}$  between carbon surface and  $\text{SiO}_2$  substrate has been estimated from molecular dynamics and is  $\approx 60 \text{ MW/Km}^2$ ,<sup>55</sup> and can depend also on the surface roughness. Alternatively, energy can be transferred directly to the substrate via the SPP phonons, i.e.,  $\kappa_{\text{SPP}}$ , and can depend sensitively on doping. For an undoped graphene,  $\kappa_{\text{SPP}}$  is on the order of  $1 \text{ MW/Km}^2$ , while  $\kappa_{\text{LAT}}$  is even smaller, as we will see later in the discussion. In this section, we discuss how

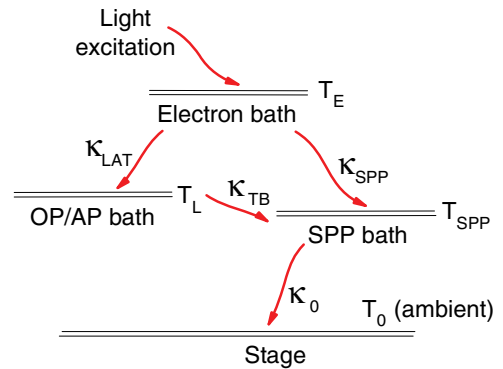


FIG. 1. (Color online) Cartoon illustrating the typical cooling pathways of hot electrons produced by continuous photoexcitation of graphene with detail descriptions in the main text. Heat can also be dissipated through metallic contacts attached to graphene (not shown), as discussed in Sec. III B.

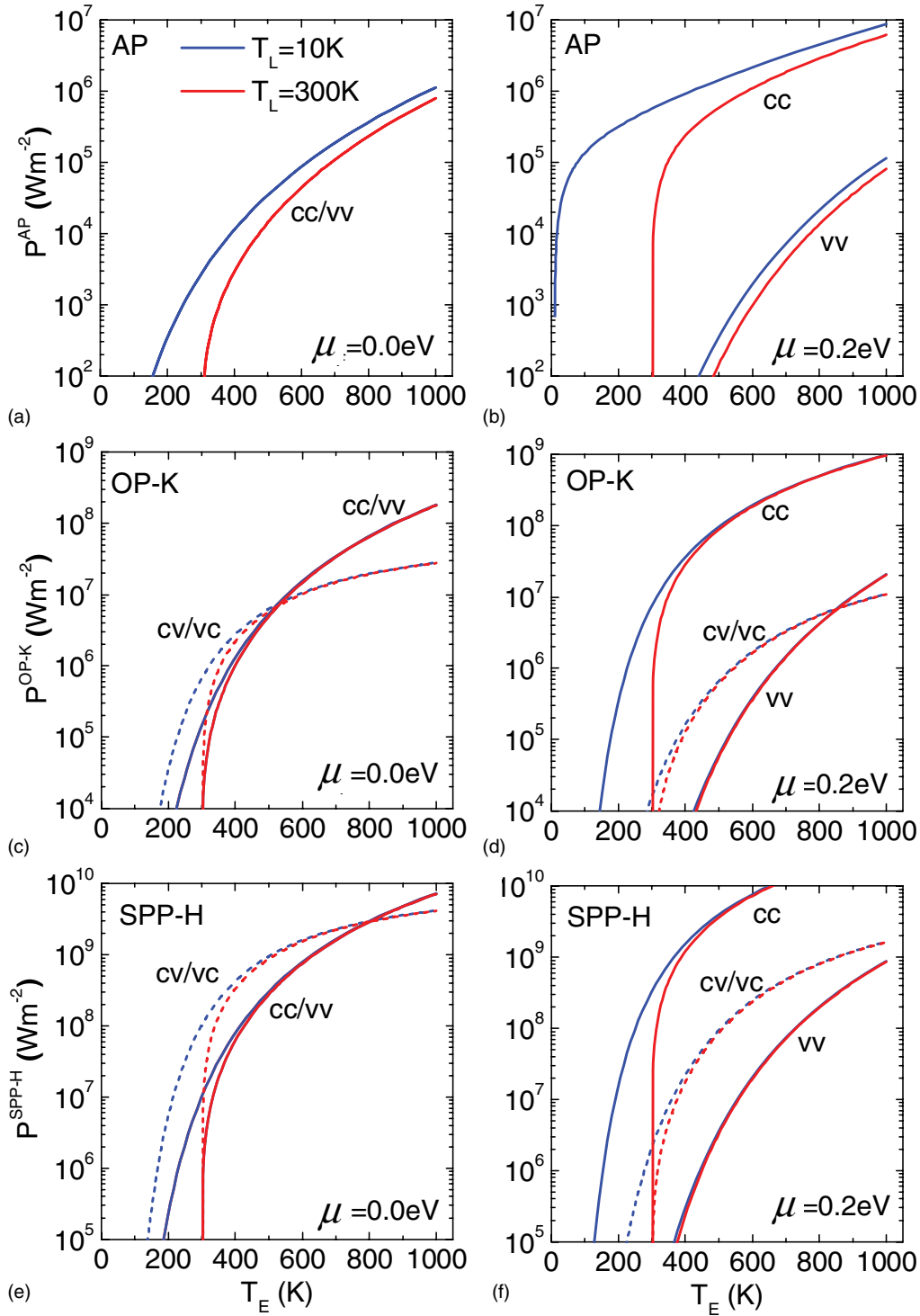


FIG. 2. (Color online) (a), (b) Electron cooling power due to acoustic phonons bath  $\mathcal{P}^{\text{AP}}$  as function of electron temperature  $T_E$  for different lattice temperature  $T_L$  calculated for neutral and doped graphene, respectively. Intraband ( $cc$ ,  $vv$ ) and interband ( $cv$ ,  $vc$ ) processes are indicated. (c), (d) Similar, except for  $K$  optical phonons modes  $\mathcal{P}^{\text{OP},K}$  and (e), (f) for high-energy *unscreened* SPP mode  $\mathcal{P}^{\text{SPP},H}$ .  $\Gamma$  optical and the low-energy SPP phonons show similar characteristics (not shown).

these cooling pathways depend on the various experimental conditions.

Detailed balance condition of in- and out-scattering processes requires that  $\mathcal{P}^\alpha$  vanishes under equilibrium condition, i.e.,  $\delta T \equiv T_E - T_L = 0$ . In the theory, this is ensured by

the composite Fermi-boson distribution function  $\mathcal{F}(T_E, T_L)$ . The energy exchange efficiency with these various phonon baths depends upon, among other factors, the doping and electronic/lattice temperatures. Using the models described in Sec. II, we calculate  $\mathcal{P}^\alpha(T_E)$  due to the various phonon

baths for intrinsic/doped graphene under cold/hot (defined at  $T_L = 10$  and 300 K, respectively) lattice temperature as shown in Fig. 2.

First, we discuss results on intrinsic graphene [see Figs. 2(a), 2(c), and 2(e)], which can be understood on the basis of scattering phase-space arguments. For cold neutral graphene, Pauli blocking limits the electronic transitions involved to mainly interband processes. Hence, under near equilibrium condition, i.e.,  $\delta T$  being small, we observed that the cooling power is mainly dominated by interband processes by optical and SPP modes. Increasing the electronic temperature alleviates Pauli blocking, and allows for intraband processes to take place. As  $\delta T$  increases further, we observe that intraband cooling begins to dominate over the interband counterpart. The efficiency of energy exchange can be explained by the electron-phonon occupation number, quantified by the composite distribution function  $\mathcal{F}(T_E, T_L)$  defined in Eq. (3). For inelastic processes, one can show that  $\mathcal{F}(T_E, T_L)$  is independent of  $T_L$  when  $\delta T \rightarrow \infty$ . This is as reflected in Fig. 2 for  $\mathcal{P}^{OP, K}$  and  $\mathcal{P}^{SPP, H}$ . On the other hand, for quasielastic acoustic phonons, the cooling power is proportional  $\delta T/T_E$  instead.

The results on doped graphene are shown in Figs. 2(b), 2(d), and 2(f). Contrary to the intrinsic case, Pauli blocking promotes intraband electronic transitions over interband processes in doped graphene. In addition,  $\mathcal{P}_{cc}^\alpha \neq \mathcal{P}_{vv}^\alpha$ , with larger cooling power for the majority carriers. At moderate doping of  $\mu = 0.2$  eV, their cooling power differs by more than an order of magnitude. The reduced electron-hole symmetry upon doping also leads to smaller interband cooling power. Quasielasticity of acoustic phonon scattering results in a phase-space restriction in the scattering, with a Bloch-Grüneisen temperature determined by the doping,<sup>45,60</sup> i.e.,  $T_{BG} = 2\hbar v_s k_F / k_B$ , in contrast to normal metals. This increase in phase space in conjunction with Pauli blocking greatly enhances the cooling power due to AP over the optical phonon baths. In fact, for moderate  $T_E \lesssim 100$  K,  $\mathcal{P}^{AP}$  dominates over all other mechanisms for cold graphene.

The lattice temperature  $T_L$  also plays an important role in the competing cooling pathways. Figure 3 compares the fractional cooling powers  $\mathcal{P}^\alpha/\mathcal{P}^T$  for intrinsic graphene, where  $\mathcal{P}^T = \sum_\alpha \mathcal{P}^\alpha$ . To obtain a quantitative estimate, we include in-plane screening of the SPP scattering potential in graphene. The screening is incorporated through a standard procedure<sup>61</sup>  $|M_{\mathbf{k}, \mathbf{k}'}| \rightarrow |M_{\mathbf{k}, \mathbf{k}'}|/\epsilon_{2D}(\mathbf{q}, \omega)$ . For simplicity, we employed the static screening dielectric function  $\epsilon_{2D}(\mathbf{q}, 0)$ , which in the long-wavelength limit assumes a simple form<sup>62</sup>  $\epsilon_{2D}(\mathbf{q}, 0) \approx 1 + q_s/q$ , where  $q_s = e^2/2\epsilon_0\kappa \int \frac{\partial f}{\partial \epsilon} \mathcal{D}(\epsilon) d\epsilon$  and  $\mathcal{D}$  is graphene density of states.  $f$  is the Fermi distribution function and is a function of the electronic temperature.

We analyze the results in two nonequilibrium temperature limits, namely, “near equilibrium” ( $T_E - T_L = 10$  K) and “far from equilibrium” ( $T_E - T_L = 100$  K) conditions. Figure 3(a) considers the condition of near equilibrium. At low  $T_L$ , AP dominates cooling. Increasing  $T_L$  populates the low-energy SPP mode, which begins to overtake the cooling power at a temperature of  $\sim 20$  K. This transition temperature increases with doping, e.g., is  $\sim 50$  K at a doping of 0.1 eV. The low-energy SPP mode is overtaken by its high-energy mode at  $\sim 170$  K. A downturn in the high-energy SPP cooling power is

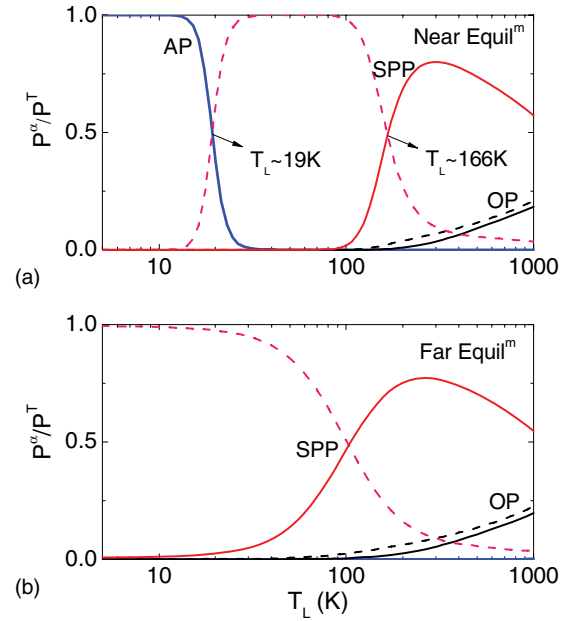


FIG. 3. (Color online) (a) Fractional cooling power  $\mathcal{P}^\alpha/\mathcal{P}^T$  where  $\mathcal{P}^T = \sum_\alpha \mathcal{P}^\alpha$ , calculated at “near-equilibrium” condition of  $T_E - T_L = 10$  K for neutral graphene, including 2D screening  $\epsilon_{2D}(q)$  described in text. For SPP and OP, the dashed (solid) line represents the low- (high-) energy mode. (b) Same as (a), except calculated for “far-from-equilibrium” condition of  $T_E - T_L = 100$  K.

observed due to larger screening at higher temperatures. Eventually, the optical phonons overtake the SPP for temperatures larger than 1000 K. Figure 3(b) considers the condition of far from equilibrium. In this case, the SPP dominates the cooling power for all  $T_L$ , except at temperature  $> 1000$  K where optical phonons begin to overtake it.

## B. Cooling dynamics

We are interested in the role played by these various phonon baths on the cooling dynamics of photoexcited carriers, more specifically, the temporal evolution of  $T_E$ . The acoustic and optical phonon baths can each establish a different temperature upon interactions with the electrons, but processes such as anharmonic phonon-phonon scattering serve to thermalize them on a picosecond time scale.<sup>3,63–65</sup> In this work, we shall assume a common lattice temperature  $T_L$ , but acknowledge that in experiments with ultrafast pump probe, this will not hold true. On the other hand, under continuous light excitation, coupling to the heat sink via the supporting substrate substantially cools the lattice temperature to within a few degrees Kelvin of the ambient temperature  $T_0$  under usual photoexcitation conditions.<sup>66</sup> Typically,  $T_E - T_L \gg 1$  K under low/moderate excitation power levels used in our studies. In this regard, the relatively small differences among the various phonon baths can be safely ignored.

Hot carrier dynamics can be probed through optical measurements.<sup>1–3,67</sup> Following a pulsed light excitation, the temporal evolution of carrier relaxation, quantified by its electronic temperature  $T_E$ , can be measured using differential transmission spectroscopy. The electron dynamics are usually

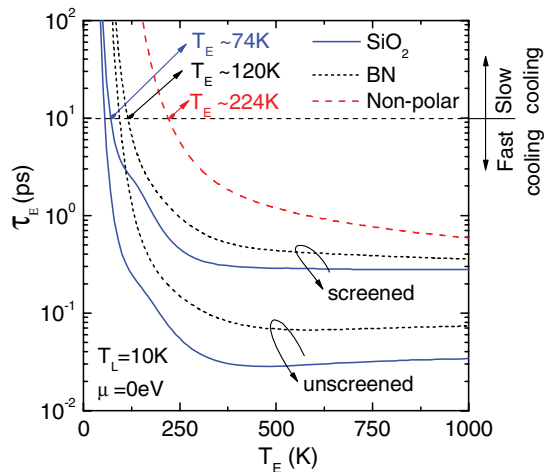


FIG. 4. (Color online) Carrier's cooling time  $\tau_E$  after photoexcitation plotted as a function of  $T_E$  calculated for cold neutral graphene. Various substrates are considered, namely,  $\text{SiO}_2$ , BN, and nonpolar, calculated for screened and unscreened SPP scattering potentials. Dotted line distinguishing fast/slow cooling is rather arbitrary, and serves only as guide to the eye.

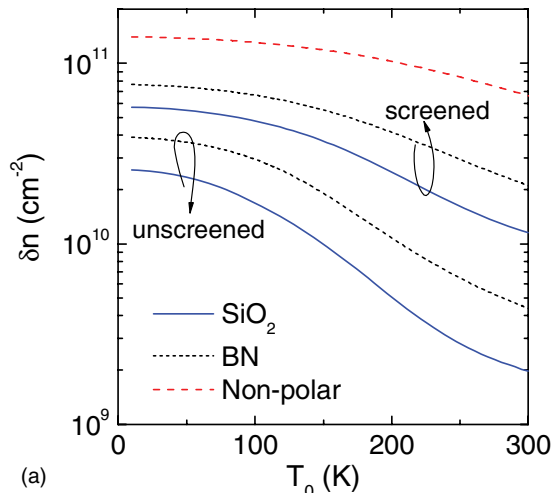
described by  $\Delta T_E \propto \exp(-t/\tau_E)$ , and can be estimated with<sup>68</sup>

$$\tau_E = C \left( \frac{d\mathcal{P}^T}{dT_E} \right)^{-1}, \quad (4)$$

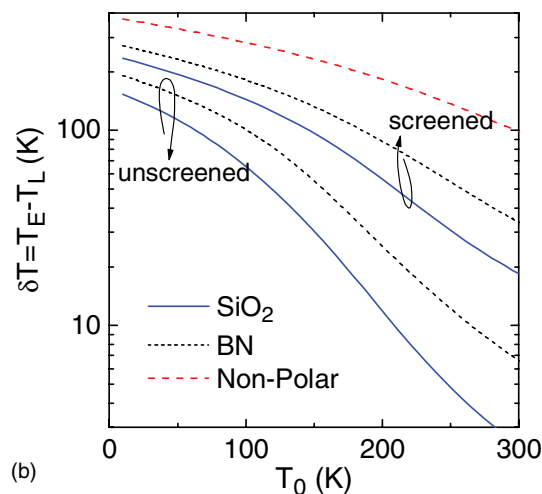
where  $C = d\mathcal{E}/dT_E$  is the electron specific heat and  $\mathcal{E}$  is the energy density of graphene. In this work,  $C$  is computed numerically. However, we note that for  $T_E \ll \mu/k_B$ ,  $C$  increases linearly with  $T_E$ , i.e.,  $C \approx \frac{2\pi^2}{3} \mathcal{D}(\mu) k_B^2 T_E$ . Having computed the total cooling power  $\mathcal{P}^T$  in Sec. III,  $\tau_E$  can be obtained directly from Eq. (4).

Figure 4 plots the cooling time  $\tau_E$  for neutral graphene at  $T_L = 10$  K. It is calculated for common substrates such as  $\text{SiO}_2$ , BN, and nonpolar substrate such as diamond. At very hot electron temperatures, i.e.,  $T_E > 500$  K,  $\tau_E$  is given by a relatively constant subpicosecond cooling time. This is in agreement with experiments.<sup>22</sup> The constancy of  $\tau_E$  suggests the  $\exp(-t/\tau_E)$  decay characteristics are typical during the initial fast cooling process. As  $T_E$  cools down, the cooling bottleneck due to AP begins to set in, leading to much slower cooling times. The transition temperature into this slow cooling regime varies with the choice of substrate as indicated in Fig. 4. This transition temperature is dictated by the lowest-frequency SPP mode of the substrate. Unscreened results, which overestimate the SPP cooling power, yield much shorter cooling lifetimes than experimentally reported.<sup>22</sup> We also note that inclusion of disorder-assisted cooling<sup>68</sup> might enhance the decay rate, especially in the slow cooling regime.

The optoelectronic response in graphene, photovoltaic<sup>69-71</sup> or thermoelectric,<sup>22,72,73</sup> is also a measure of the energy transport of these hot carriers. These experiments are usually performed under a continuous light illumination of an electrostatic junction. Their relative contribution depends on the electrostatic junction characteristics, doping, and even extrinsic factors such as electron-hole puddles.<sup>74</sup> Nevertheless, at steady state, the photovoltaic current is proportional to the photogenerated excess carrier density  $\delta n$  via  $e\delta n\mu_n\xi$



(a)



(b)

FIG. 5. (Color online) (a) Steady-state excess carrier density  $\delta n$  upon continuous photoexcitation as a function of the ambient temperature for neutral graphene. Various substrates are considered, namely,  $\text{SiO}_2$ , BN, and nonpolar, calculated for screened and unscreened SPP scattering potentials. (b) Elevated temperatures  $T_E - T_L$ , calculated for same conditions in (a). All calculations assumed  $\mathcal{P}^0 = 1 \times 10^7$  W/m<sup>2</sup> and  $\kappa_0 = 10$  MW/Km<sup>2</sup>.

where  $\mu_n$  is the carrier mobility and  $\xi$  the local electric field. The thermoelectric response, on the other hand, is proportional to the local elevated temperature  $\delta T = T_E - T_L$  via  $\sigma(S_1 - S_2)\delta T$  where  $S_{1,2}$  is the Seebeck coefficient of the two junction and  $\sigma$  is the device conductivity. Here, we discuss estimates of  $\delta n$  and  $\delta T$ .

Under steady-state condition,

$$\mathcal{P}^0 = \sum_{\alpha} \mathcal{P}^{\alpha} + \mathcal{P}^M, \quad (5)$$

where  $\mathcal{P}^0$  is the laser power absorbed by graphene, and  $\mathcal{P}^M$  is the heat dissipation via the metallic contacts, if any. In the absence of contacts, all heat dissipation is via the supporting substrate. At steady state,  $\mathcal{P}^{\text{AP}} + \mathcal{P}^{\text{OP}} + \mathcal{P}^{\text{SPP}} \approx (T_L - T_0)\kappa_0$ . Equation (5) is then solved self-consistently in conjunction with charge conservation, i.e.,  $\delta n = n_e(T_E, \mu) - n_e(T_0, \mu_0) = n_h(T_E, \mu) - n_h(T_0, \mu_0)$ , arriving at steady-state values for  $T_E$  and  $\mu$ . The photoexcited carrier density  $\delta n$  and the elevated

temperature  $\delta T$  are plotted in Figs. 5(a) and 5(b), respectively, assuming typical experimental values of  $\mathcal{P}^0 = 1 \times 10^7 \text{ W/m}^2$  and  $\kappa_0 = 10 \text{ MW/Km}^2$ . Both  $\delta n$  and  $\delta T$  decrease with increasing ambient temperature  $T_0$ , due to more efficient cooling as phonon occupation increases. For  $\text{SiO}_2$ ,  $\delta n \approx 10^{10} \text{ cm}^{-2}$  and  $\delta T \approx 10 \text{ K}$  under room-temperature condition, of the same order typically seen in measurement.<sup>66</sup> Increasing doping increases the scattering phase space for intraband processes and leads to more efficient electronic cooling into the phonon baths, as shown in Fig. 2. As a result, both  $\delta n$  and  $\delta T$  decrease with increasing doping.

We also estimate the heat dissipation via contacts phenomenologically with  $\mathcal{P}^M \approx \int (f - f_0)(E - \mu) \mathcal{D} / \tau_M dE$  where  $f_0$  is the distribution function before light excitation. First, we consider the simple ballistic limit where  $\tau_M$  is just the device lifetime given by  $L/v_F$ , where  $L$  is the length of the device and  $v_F \approx 10^6 \text{ m/s}$  is the Fermi velocity. Here, we assume a typical  $\tau_M = 1 \text{ ps}$ . We found that including  $\mathcal{P}^M$  only leads to fewfold decrease in the quantitative results presented in Fig. 5 (not shown). In the realistic case where the carrier transport is in the diffusive dominated regime,  $\mathcal{P}^M$  would be even smaller, by a factor of  $\lambda/L$ , where  $\lambda$  is the carrier's mean-free path.

Figure 5 also suggests an order-of-magnitude enhancement in the optoelectronic response of graphene, by suppressing the SPP heat dissipation through a nonpolar substrate, such as diamondlike carbon,<sup>75</sup> or by suspending graphene. In fact, the amount of heat transfer to the substrate via the electron coupling with the SPP can be quantified by an out-of-plane thermal conductance  $\kappa_{\text{SPP}}$ , defined as  $\kappa_{\text{SPP}} = \mathcal{P}^{\text{SPP}} / \delta T$ . This quantity sets the lower limit on the interfacial thermal conductance and it is plotted in Fig. 6. At room temperature,  $\kappa_{\text{SPP}} \approx 1 \text{ MW/Km}^2$  for undoped graphene, and can increase with doping to order of  $10 \text{ MW/Km}^2$  (see also Ref. 59). For typical photocurrent experiments,  $L$  is typically  $\gg \lambda$ , and transport is in the diffusive

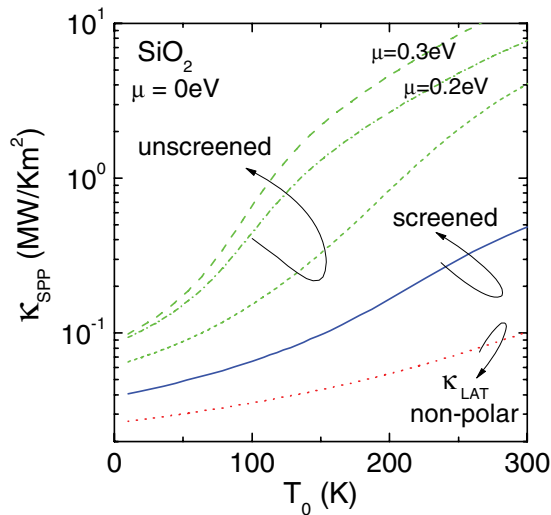


FIG. 6. (Color online) Out-of-plane thermal conductance  $\kappa_{\text{SPP}}$  defined as  $\kappa_{\text{SPP}} = \mathcal{P}^{\text{SPP}} / \delta T$  calculated for  $\text{SiO}_2$  for different conditions such as (i) screened and unscreened SPP scattering potentials and (ii) different doping  $\mu$  (all curves are for zero doping unless stated otherwise).  $\kappa_{\text{LAT}}$  for undoped graphene on a nonpolar substrate is plotted as reference.

regime. Here, the in-plane electronic thermal conductivity  $\kappa_e$  can be estimated from the Wiedemann-Franz relation. We found that our estimated value of  $\kappa_{\text{SPP}}$  is significantly larger than  $\kappa_e/L^2$  for typical experimental situations. This suggests that out-of-plane heat dissipation via SPP dominates over the in-plane electronic heat conduction. The former leads to an increased temperature of the graphene lattice. This result reconciles with recent experiment,<sup>66</sup> which reveals significant lattice heating upon laser excitation. From the experiment,<sup>66</sup> we can estimate an out-of-plane thermal conductance of  $\kappa_{\text{exp}} = \mathcal{P}^0 / \delta T \approx 10 \text{ MW/Km}^2$ . This value is consistent with our estimated  $\kappa_{\text{SPP}}$ . In fact,  $\kappa_{\text{LAT}}$  alone is orders of magnitude smaller than the experiment as shown in Fig. 6.

#### IV. CONCLUSIONS

Our results point to the limiting role played by remote substrate phonons in the energy relaxation of hot photocarriers. In particular, we have shown that the steady-state photoreponse in graphene is controlled by the inelastic scattering. The photovoltaic current is proportional to the photogenerated excess carrier density. The thermoelectric contribution, on the other hand, is proportional to the elevated electron temperature. Our results show that irrespective of the mechanism, the SPP phonons limit the overall strength of the photocurrent response on polar substrates. We predict that a choice of a nonpolar substrate will lead to an order-of-magnitude enhancement in graphene photoresponse. Therefore, substrate engineering presents a promising route to efficient optoelectronic devices driven by hot carrier dynamics.

#### ACKNOWLEDGMENTS

T.L. acknowledges use of a computing cluster provided by Network for Computational Nanotechnology, partial funding from INDEX-NRI and in part by the NSF under Grant No. NSF PHY05-51164 (KITP). We thank F. Xia, H. Yan, F. Guinea, E. Hwang, and X. Xu for useful discussions.

#### APPENDIX A: ACOUSTIC PHONON

We consider first the energy exchange with the acoustic phonon (AP) bath. The total matrix element for electron-acoustic phonon scattering due to the two acoustic phonon modes, i.e.,  $\Gamma_{\text{LA}}$  and  $\Gamma_{\text{TA}}$ , is given by<sup>33,45</sup>

$$|M_{\mathbf{k},\mathbf{k}'}^{\text{AP}}|^2 = \frac{D_{ac}^2 \hbar q}{2\rho_m v_S}, \quad (\text{A1})$$

where  $D_{ac}$  is the acoustic deformation potential, taken to be 7.1 eV in our calculations, which is very similar to the recent *ab initio* calculations of 6.8 eV.<sup>76</sup> We note that the electron-phonon matrix element for these two acoustic modes has different angular dependencies with transition matrix elements,<sup>76,77</sup> which became negated after summing them.<sup>77</sup>  $v_S$  is graphene effective sound velocity defined as<sup>33</sup>  $2v_S^{-2} = v_{\text{LA}}^{-2} + v_{\text{TA}}^{-2}$ , where  $v_S = 17 \text{ km/s}$ ,  $v_{\text{LA}} = 24 \text{ km/s}$ , and  $v_{\text{TA}} = 14 \text{ km/s}$ .  $\rho_m$  is graphene mass density taken to be

$7.6 \times 10^{-7} \text{ kg/m}^2$ . The acoustic phonon is then described by an effective Debye linear dispersion  $\omega_q = v_S q$ . Since  $v_S \ll v_F$ ,  $\hbar\omega_q$  is typically much smaller than the other energy scale in the problem. The acoustic phonon scattering is thus approximated to be elastic,<sup>19</sup> i.e.,  $k' \approx k$ .

The cooling power can then be written as

$$\begin{aligned} \mathcal{P}_{cc}^{\text{AP}} &= \frac{g_s g_v}{(2\pi)^2 \hbar} \int_0^\infty k dk \int_0^\infty k' dk' \int_0^{2\pi} d\theta \frac{D_{ac}^2 \hbar q}{2\rho_m v_S} \\ &\times \delta(k' - k - \omega_q v_F^{-1})(k' - k) \mathcal{F}(k, k') \\ &\approx \frac{g_s g_v}{(2\pi)^2 \hbar} \frac{D_{ac}^2 \hbar}{2\rho_m v_S} \int_0^\infty \int_0^{2\pi} k^2 q^2 \frac{v_S}{v_F} \mathcal{F}(k, k) dk d\theta. \quad (\text{A2}) \end{aligned}$$

Under the assumption  $\hbar\omega_q \ll T_E, T_L$ , we have

$$\mathcal{F}(k, k) \approx (1 - f_k) f_k \frac{T_E - T_L}{T_E}. \quad (\text{A3})$$

Making use of the relations  $q^2 \approx 2k^2(1 - \cos\theta)$ , we then obtain a simplified form for the cooling power,

$$\mathcal{P}_{cc}^{\text{AP}} \approx \frac{g_s g_v D_{ac}^2}{2\pi \rho_m v_S} \frac{T_E - T_L}{T_E} \int_0^\infty k^4 (1 - f_k) f_k dk. \quad (\text{A4})$$

Contributions from interband processes  $\mathcal{P}_{cv}^{\text{AP}}$  are forbidden due to energy-momentum conservations.

## APPENDIX B: OPTICAL PHONONS

Next, we discuss energy exchanges with high-energy dispersionless optical phonon (OP) modes, i.e.,  $\Gamma_{\text{LO}}$ ,  $\Gamma_{\text{TO}}$ , and  $\text{K}_{\text{TO}}$ . We consider first the electron-phonon coupling of long-wavelength optical phonon modes  $\Gamma_{\text{LO}}$  and  $\Gamma_{\text{TO}}$ . Their sum is expressed as<sup>46,47</sup>

$$|M_{\mathbf{k}, \mathbf{k}'}^{\text{OP}, \Gamma}|^2 = \frac{\hbar D_{\text{OP}, \Gamma}^2}{2\rho_m \omega_o}, \quad (\text{B1})$$

where  $D_{\text{OP}, \Gamma} = 3\sqrt{2}g/2 \approx 11 \text{ eV \AA}^{-1}$  is the optical-phonon deformation potential with a coupling constant of  $g = 5.3 \text{ eV \AA}^{-1}$ , and  $\hbar\omega_o = 197 \text{ meV}$ . We note that the electron-phonon matrix element for these two optical modes has different angular dependencies with transition matrix elements,<sup>46,47</sup> i.e.,  $1 \pm s s' \cos(\theta_{\mathbf{k}} - \theta_{\mathbf{k}'})$  where  $s = \pm 1$  denotes conduction/valence bands, which again became negated after summing them.

We consider first the intraband cooling power, written as

$$\begin{aligned} \mathcal{P}_{cc}^{\text{OP}, \Gamma} &= \frac{g_s g_v}{(2\pi)^2 \hbar} \int_0^\infty k dk \int_0^\infty k' dk' \int_0^{2\pi} d\theta \frac{D_{\text{OP}, \Gamma}^2 \hbar}{2\rho_m \omega_o} \\ &\times \delta(k' - k - \omega_o v_F^{-1})(k' - k) \mathcal{F}(k, k') \\ &= \frac{g_s g_v D_{\text{OP}, \Gamma}^2}{4\pi \rho_m v_F} \int_0^\infty k(k + \omega_o v_F^{-1}) \mathcal{F}(k, k + \omega_o v_F^{-1}) dk \\ &= \frac{g_s g_v D_{\text{OP}, \Gamma}^2}{4\pi \rho_m v_F} N_{\omega_o} \left[ \exp\left(\frac{\hbar\omega_o}{k_B T_L}\right) - \exp\left(\frac{\hbar\omega_o}{k_B T_E}\right) \right] \\ &\times \int_0^\infty k(k + \omega_o v_F^{-1})(1 - f_k) f_{k + \omega_o v_F^{-1}} dk. \quad (\text{B2}) \end{aligned}$$

In similar fashion, the interband cooling power is written as

$$\begin{aligned} \mathcal{P}_{cv}^{\text{OP}, \Gamma} &= \frac{g_s g_v D_{\text{OP}, \Gamma}^2}{4\pi \rho_m v_F} N_{-\omega_o} \left[ \exp\left(\frac{-\hbar\omega_o}{k_B T_L}\right) - \exp\left(\frac{-\hbar\omega_o}{k_B T_E}\right) \right] \\ &\times \int_0^\infty k(\omega_o v_F^{-1} - k) H_v[\omega_o v_F^{-1} - k] \\ &\times (1 - f_k) f_{k - \omega_o v_F^{-1}} dk, \quad (\text{B3}) \end{aligned}$$

where  $H_v$  is the Heaviside function.

For zone-edge phonon modes, only the transverse  $\text{K}_{\text{TO}}$  contributes to carrier scattering, and the matrix element is<sup>46</sup>

$$|M_{\mathbf{k}, \mathbf{k}'}^{\text{OP}, \text{K}}|^2 = \frac{\hbar D_{\text{OP}, \text{K}}^2}{2\rho_m \omega_o} \frac{1 - s s' \cos\theta}{2}, \quad (\text{B4})$$

where  $D_{\text{OP}, \text{K}} = 3g \approx 16 \text{ eV \AA}^{-1}$  and  $\hbar\omega_o = 157 \text{ meV}$ . The cooling power is similar to the  $\Gamma$  phonons case, except a factor of  $\frac{1}{2}$  smaller due to the angular dependence.

## APPENDIX C: SURFACE POLAR PHONONS

The surface polar phonons coupling is given by<sup>26,32,33</sup>

$$|M_{\mathbf{k}, \mathbf{k}'}^{\text{SPP}}|^2 = \frac{\pi e^2}{\epsilon_0} F_j^2 \frac{\exp(-2qz_0)}{q} \frac{1 + s s' \cos\theta}{2}, \quad (\text{C1})$$

where  $\epsilon_0$  is the free-space permittivity and  $z_0$  is the separation between graphene and the substrate. The magnitude of the polarization field is given by the Frohlich coupling parameter  $F_j^2$ . In common  $\text{SiO}_2$  dielectrics, there are two dominant surface optical phonon modes having energies  $\hbar\omega_1 = 58.9 \text{ meV}$  and  $\hbar\omega_2 = 156.4 \text{ meV}$ , with Frohlich coupling  $F_1^2 = 0.237 \text{ meV}$  and  $F_2^2 = 1.612 \text{ meV}$ , respectively.<sup>33</sup>

We consider first the intraband cooling power, written as

$$\begin{aligned} \mathcal{P}_{cc}^{\text{SPP}} &= \frac{g_s g_v}{(2\pi)^2 \hbar} \int_0^\infty k dk \int_0^\infty k' dk' \int_0^{2\pi} d\theta \frac{\pi e^2}{\epsilon_0} F_j^2 \frac{\exp(-2qz_0)}{q} \frac{1 + s s' \cos\theta}{2} \delta(k' - k - \omega_j v_F^{-1})(k' - k) \mathcal{F}(k, k') \\ &= \frac{g_s g_v}{(2\pi)^2 \hbar} \frac{\omega_j}{v_F} \frac{\pi e^2}{\epsilon_0} F_j^2 \int_0^\infty k(k + \omega_j v_F^{-1}) \mathcal{F}(k, k + \omega_j v_F^{-1}) \int_0^{2\pi} \frac{\exp(-2qz_0)}{q} \frac{1 + \cos\theta}{2} d\theta dk. \quad (\text{C2}) \end{aligned}$$

The phonon momentum  $q$  has the constraint  $q^2 = k'^2 + k^2 - 2k'k\cos\theta$ . Under typical conditions, the factor  $\exp(-2qz_0) \approx 1$ . Linearizing  $\exp(-2qz_0)$ , the intraband cooling power then becomes

$$\mathcal{P}_{cc}^{\text{SPP}} = \frac{g_s g_v \omega_j \pi e^2 F_j^2}{(2\pi)^2 \hbar v_F \epsilon_0} N_{\omega_j} \left[ \exp\left(\frac{\hbar\omega_j}{k_B T_L}\right) - \exp\left(\frac{\hbar\omega_j}{k_B T_E}\right) \right] \int_0^\infty k k' (1 - f_k) f_{k'} \Theta(k, k') \exp\left(\frac{-z_0}{\Theta(k, k')}\right) dk, \quad (\text{C3})$$

where  $k' \equiv k + \omega_0 v_F^{-1}$  and

$$\Theta(k, k') \equiv \int_0^{2\pi} \frac{1 + \cos\theta}{2\sqrt{k'^2 + k^2 - 2kk'\cos\theta}} d\theta \\ = \frac{k + k'}{kk'} \left[ I_K \left( \frac{2\sqrt{kk'}}{k + k'} \right) - I_E \left( \frac{2\sqrt{kk'}}{k + k'} \right) \right], \quad (\text{C4})$$

where  $I_{K,E}$  are the complete elliptic integrals of first and second kind. In similar fashion, the interband cooling power

is written as

$$\mathcal{P}_{cv}^{\text{SPP}} = \frac{g_s g_v \omega_j \pi e^2 F_j^2}{(2\pi)^2 \hbar v_F \epsilon_0} N_{-\omega_j} \left[ \exp \left( \frac{-\hbar\omega_j}{k_B T_L} \right) - \exp \left( \frac{-\hbar\omega_j}{k_B T_E} \right) \right] \\ \times \int_0^\infty kk' H_v[k'](1 - f_k) f_{-k'} \Theta(k, -k') \\ \times \exp \left( \frac{-z_0}{\Theta(k, -k')} \right) dk, \quad (\text{C5})$$

where  $k' \equiv \omega_0 v_F^{-1} - k$ .

\*Present address: Components Research, Intel Corporation, Hillsboro, OR 97124, USA.

- <sup>1</sup>D. Sun, Z. K. Wu, C. Divin, X. Li, C. Berger, W. A. de Heer, P. N. First, and T. B. Norris, *Phys. Rev. Lett.* **101**, 157402 (2008).
- <sup>2</sup>J. M. Dawlaty, S. Shivaraman, M. Chandrashekhara, F. Rana, and M. G. Spencer, *Appl. Phys. Lett.* **92**, 042116 (2008).
- <sup>3</sup>T. Kampfrath, L. Perfetti, F. Schapper, C. Frischkorn, and M. Wolf, *Phys. Rev. Lett.* **95**, 187403 (2005).
- <sup>4</sup>M. Breusing, C. Ropers, and T. Elsaesser, *Phys. Rev. Lett.* **102**, 086809 (2009).
- <sup>5</sup>M. Breusing, S. Kuehn, T. Winzer, E. Malic, F. Milde, N. Severin, J. P. Rabe, C. Ropers, A. Knorr, and T. Elsaesser, *Phys. Rev. B* **83**, 153410 (2011).
- <sup>6</sup>R. W. Newson, J. Dean, B. Schmidt, and H. M. van Driel, *Opt. Exp.* **17**, 2326 (2009).
- <sup>7</sup>H. Choi, F. Borondics, D. A. Siegel, S. Y. Zhou, M. C. Martin, A. Lanzara, and R. A. Kaindl, *Appl. Phys. Lett.* **94**, 172102 (2009).
- <sup>8</sup>H. Wang, J. H. Strait, P. A. George, S. Shivaraman, V. B. Shields, M. Chandrashekhara, J. Hwang, F. Rana, M. G. Spencer, C. S. Ruiz-Vargas *et al.*, *Appl. Phys. Lett.* **96**, 081917 (2010).
- <sup>9</sup>P. A. George, J. Strait, J. Dawlaty, S. Shivaraman, M. Chandrashekhara, F. Rana, and M. G. Spencer, *Nano Lett.* **8**, 4248 (2008).
- <sup>10</sup>S. Kumar, M. Anija, N. Kamaraju, K. S. Vasu, K. S. Subrahmanyam, A. K. Sood, and C. N. R. Rao, *Appl. Phys. Lett.* **95**, 191911 (2009).
- <sup>11</sup>K. Ishioka, M. Hase, M. Kitajima, L. Wirtz, A. Rubio, and H. Petek, *Phys. Rev. B* **77**, 121402 (2008).
- <sup>12</sup>K. Seibert, G. C. Cho, W. Kütt, H. Kurz, D. H. Reitze, J. I. Dadap, H. Ahn, M. C. Downer, and A. M. Malvezzi, *Phys. Rev. B* **42**, 2842 (1990).
- <sup>13</sup>S. Winnerl, M. Orlita, P. Plochocka, P. Kossacki, M. Potemski, T. Winzer, E. Malic, A. Knorr, M. Sprinkle, C. Berger *et al.*, *Phys. Rev. Lett.* **107**, 237401 (2011).
- <sup>14</sup>T. Winzer, A. Knorr, and E. Malic, *Nano Lett.* **10**, 4839 (2010).
- <sup>15</sup>R. Kim, V. Perebeinos, and P. Avouris, *Phys. Rev. B* **84**, 075449 (2011).
- <sup>16</sup>E. Malic, T. Winzer, E. Bobkin, and A. Knorr, *Phys. Rev. B* **84**, 205406 (2011).
- <sup>17</sup>T. Hertel and G. Moos, *Phys. Rev. Lett.* **84**, 5002 (2000).
- <sup>18</sup>C. H. Lui, K. F. Mak, J. Shan, and T. F. Heinz, *Phys. Rev. Lett.* **105**, 127404 (2010).
- <sup>19</sup>R. Bistritzer and A. H. MacDonald, *Phys. Rev. Lett.* **102**, 206410 (2009).
- <sup>20</sup>W. K. Tse and S. Das Sarma, *Phys. Rev. B* **79**, 235406 (2009).
- <sup>21</sup>S. S. Kubakaddi, *Phys. Rev. B* **79**, 075417 (2009).
- <sup>22</sup>D. Sun, G. Aivazian, A. M. Jones, J. S. Ross, W. Yao, D. Cobden, and X. Xu, *Nat. Nanotechnol.* **7**, 114 (2012).
- <sup>23</sup>N. W. Ashcroft and D. N. Mermin, *Solid State Physics* (Harcourt-Brace, New York, 1976), p. 27.
- <sup>24</sup>S. Q. Wang and G. D. Mahan, *Phys. Rev. B* **6**, 4517 (1972).
- <sup>25</sup>K. Hess and P. Vogl, *Solid State Commun.* **30**, 807 (1979).
- <sup>26</sup>M. V. Fischetti, D. A. Neumayer, and E. A. Cartier, *J. Appl. Phys.* **90**, 4587 (2001).
- <sup>27</sup>A. G. Petrov and S. V. Rotkin, *JETP Lett.* **84**, 156 (2006) [*Pis'ma v ZhETF* **84**, 185 (2006)].
- <sup>28</sup>V. Perebeinos, S. V. Rotkin, A. G. Petrov, and P. Avouris, *Nano Lett.* **9**, 312 (2009).
- <sup>29</sup>B. Chandra, V. Perebeinos, S. Berciaud, J. Katoch, M. Ishigami, P. Kim, T. F. Heinz, and J. Hone, *Phys. Rev. Lett.* **107**, 146601 (2011).
- <sup>30</sup>I. Meric, M. Y. Han, A. F. Young, B. Ozyilmaz, P. Kim, and K. L. Shepard, *Nat. Nanotechnol.* **3**, 654 (2008).
- <sup>31</sup>J. H. Chen, C. Jang, S. Xiao, M. Ishigami, and M. S. Fuhrer, *Nat. Nanotechnol.* **3**, 206 (2008).
- <sup>32</sup>S. Fratini and F. Guinea, *Phys. Rev. B* **77**, 195415 (2008).
- <sup>33</sup>V. Perebeinos and P. Avouris, *Phys. Rev. B* **81**, 195442 (2010).
- <sup>34</sup>A. Konar, T. Fang, and D. Jena, *Phys. Rev. B* **82**, 115452 (2010).
- <sup>35</sup>X. Li, E. A. Barry, J. M. Zavada, M. B. Nardelli, and K. W. Kim, *Appl. Phys. Lett.* **97**, 232105 (2010).
- <sup>36</sup>A. S. Price, S. M. Hornett, A. V. Shytov, E. Hendry, and D. W. Horsell, *Phys. Rev. B* **85**, 161411(R) (2012).
- <sup>37</sup>J. Schiefele, F. Sols, and F. Guinea, *Phys. Rev. B* **85**, 195420 (2012).
- <sup>38</sup>K. Zou, X. Hong, D. Keefer, and J. Zhu, *Phys. Rev. Lett.* **105**, 126601 (2010).
- <sup>39</sup>A. M. DaSilva, K. Zou, J. K. Jain, and J. Zhu, *Phys. Rev. Lett.* **104**, 236601 (2010).
- <sup>40</sup>Y. Liu and R. F. Willis, *Phys. Rev. B* **81**, 081406 (2010).
- <sup>41</sup>Z. Fei, G. O. Andreev, W. Bao, L. M. Zhang, A. S. McLeod, C. Wang, M. K. Stewart, Z. Zhao, G. Dominguez, M. Thiemens *et al.*, *Nano Lett.* **11**, 4701 (2011).
- <sup>42</sup>J. Chen, M. Badioli, P. A. Gonzalez, S. Thongrattanasiri, F. Huth, J. Osmond, M. Spasenovic, A. Centeno, A. Pesquera, P. Godignon *et al.*, *Nature* (2012), doi: 10.1038/nature11254.
- <sup>43</sup>E. M. Conwell, *Solid State Physics Supplement* (Academic, New York, 1967).
- <sup>44</sup>S. J. Manion, M. Artaki, M. A. Emanuel, J. J. Coleman, and K. Hess, *Phys. Rev. B* **35**, 9203 (1987).
- <sup>45</sup>E. H. Hwang and S. Das Sarma, *Phys. Rev. B* **77**, 115449 (2008).
- <sup>46</sup>M. Lazzeri, S. Piscanec, F. Mauri, A. C. Ferrari, and J. Robertson, *Phys. Rev. Lett.* **95**, 236802 (2005).

- <sup>47</sup>T. Ando, *J. Phys. Soc. Jpn.* **75**, 124701 (2006).
- <sup>48</sup>R. Geick, C. H. Perry, and G. Rupprecht, *Phys. Rev.* **146**, 543 (1966).
- <sup>49</sup>T. Yamane, N. Nagai, S. Katayama, and M. Todoki, *J. Appl. Phys.* **91**, 9772 (2002).
- <sup>50</sup>A. A. Balandin, *Nat. Mater.* **10**, 569 (2011).
- <sup>51</sup>Z. Chen, W. Jang, W. Bao, C. N. Lau, and C. Dames, *Appl. Phys. Lett.* **95**, 161910 (2009).
- <sup>52</sup>M. Freitag, M. Steiner, Y. Martin, V. Perebeinos, Z. Chen, J. C. Tsang, and P. Avouris, *Nano Lett.* **9**, 1883 (2009).
- <sup>53</sup>K. F. Mak, C. H. Lui, and T. F. Heinz, *Appl. Phys. Lett.* **97**, 221904 (2010).
- <sup>54</sup>Y. K. Koh, M.-H. Bae, D. G. Cahill, and E. Pop, *Nano Lett.* **10**, 4363 (2010).
- <sup>55</sup>Z.-Y. Ong and E. Pop, *Phys. Rev. B* **81**, 155408 (2010).
- <sup>56</sup>B. N. J. Persson and H. Ueba, *Europhys. Lett.* **91**, 56001 (2010).
- <sup>57</sup>B. N. J. Persson and H. Ueba, *J. Phys. C: Solid State Phys.* **22**, 462201 (2010).
- <sup>58</sup>A. I. Volokitin and B. N. J. Persson, *Phys. Rev. B* **83**, 241407 (2011).
- <sup>59</sup>A. G. Petrov and S. V. Rotkin (unpublished).
- <sup>60</sup>D. K. Efetov and P. Kim, *Phys. Rev. Lett.* **105**, 256805 (2010).
- <sup>61</sup>D. K. Ferry and S. M. Goodnick, *Transport in Nanostructures* (Cambridge University Press, Cambridge, UK, 1997).
- <sup>62</sup>T. Ando, *J. Phys. Soc. Jpn.* **75**, 074716 (2006).
- <sup>63</sup>N. Bonini, M. Lazzeri, N. Marzari, and F. Mauri, *Phys. Rev. Lett.* **99**, 176802 (2007).
- <sup>64</sup>D. Song, F. Wang, G. Dukovic, M. Zheng, E. D. Semke, L. E. Brus, and T. F. Heinz, *Phys. Rev. Lett.* **100**, 225503 (2008).
- <sup>65</sup>H. Yan, D. Song, K. F. Mak, I. Chatzakis, J. Maultzsch, and T. F. Heinz, *Phys. Rev. B* **80**, 121403(R) (2009).
- <sup>66</sup>M. Freitag, T. Low, F. Xia, and P. Avouris, arXiv:1202.5342.
- <sup>67</sup>J. Shah, *Hot Carrier in Semiconductor Nanostructures* (Academic, London, 1992).
- <sup>68</sup>J. C. W. Song, M. Y. Reizer, and L. S. Levitov, arXiv:1111.4678.
- <sup>69</sup>F. Xia, T. Mueller, Y. M. Lin, A. V. Garcia, and P. Avouris, *Nat. Nanotechnol.* **4**, 839 (2009).
- <sup>70</sup>E. J. Lee, K. Balasubramanian, R. T. Weitz, M. Burghard, and K. Kern, *Nat. Nanotechnol.* **3**, 486 (2008).
- <sup>71</sup>J. Park, Y. H. Ahn, and C. Ruiz-Vargas, *Nano Lett.* **9**, 1742 (2009).
- <sup>72</sup>N. M. Gabor, J. C. W. Song, Q. Ma, N. L. Nair, T. Taychatanapat, K. Watanabe, T. Taniguchi, L. S. Levitov, and P. Jarillo-Herrero, *Science* **334**, 648 (2011).
- <sup>73</sup>X. Xu, N. M. Gabor, J. S. Alden, A. M. va der Zande, and P. L. McEuen, *Nano Lett.* **10**, 562 (2009).
- <sup>74</sup>J. C. W. Song, M. S. Rudner, C. M. Marcus, and L. S. Levitov, *Nano Lett.* **11**, 4688 (2011).
- <sup>75</sup>Y. Wu, Y. M. Lin, A. A. Bol, K. A. Jenkins, F. Xia, D. B. Farmer, Y. Zhu, and P. Avouris, *Nature (London)* **472**, 74 (2011).
- <sup>76</sup>K. Kaasbjerg, K. S. Thygesen, and K. W. Jacobsen, *Phys. Rev. B* **85**, 165440 (2012).
- <sup>77</sup>L. Pietronero, S. Strassler, H. R. Zeller, and M. J. Rice, *Phys. Rev. B* **22**, 904 (1980).